Article:
Conte, M., Liu, X., Murphy, D.M. et al. (3 more authors) (2016) Insights into the Reaction Mechanism of Cyclohexane Oxidation Catalysed by Molybdenum Blue Nanorings. Catalysis Letters, 146 (1). pp. 126-135. ISSN 1011-372X

https://doi.org/10.1007/s10562-015-1660-y

Insights into the reaction mechanism of cyclohexane oxidation catalysed by molybdenum blue nanorings

Marco Conte,[a,b] Xi Liu,[a] Damien M. Murphy,[a] Stuart H. Taylor,[a] Keith Whiston,[c] Graham J. Hutchings[a*]

[a] Cardiff Catalysis Institute, School of Chemistry, Cardiff University, Cardiff, CF10 3AT, UK

[b] Department of Chemistry, Dainton Building, University of Sheffield, Sheffield, S3 7HF, UK

[c] INVISTA Textiles (UK) Limited, P.O. Box 2002, Wilton, Redcar, TS10 4XX, UK

Abstract

Molybdenum blue (MB), is a polyoxometalate with a nanoring structure comprising Mo^{5+}-O-Mo^{6+} bridges, which is active for the catalytic oxidation of cyclohexane to cyclohexanol and cyclohexanone. However, little is known about the mechanistic features responsible of this catalytic activity. In the present work, the Mo^{5+}-O-Mo^{6+} moieties embedded in the MB nanoring structure were characterized using diffuse reflectance-UV-Visible spectroscopy and solid state EPR spectroscopy. The amount of Mo^{5+} centres was then varied by thermal treatment of the polyoxometalate in the absence of oxygen, and the resultant effect on the catalytic activity was investigated. It was observed that, an increased amount of Mo^{5+} centres preserved the conversion of cyclohexane (ca. 6%) but led to a loss of selectivity to cyclohexanol giving cyclohexanone as the major product, and the simultaneous formation of adipic acid. To rationalise these results the catalysts were studied using EPR spin trapping to investigate the decomposition of cyclohexyl hydroperoxide (CHHP), a key intermediate in the oxidation process of cyclohexane. This analysis showed that CHHP has to be bound to the MB surface in order to explain its catalytic activity and product distribution.

Keywords: molybdenum blue, cyclohexane oxidation, DR-UV-Vis spectroscopy, EPR spectroscopy.

Graphical Abstract

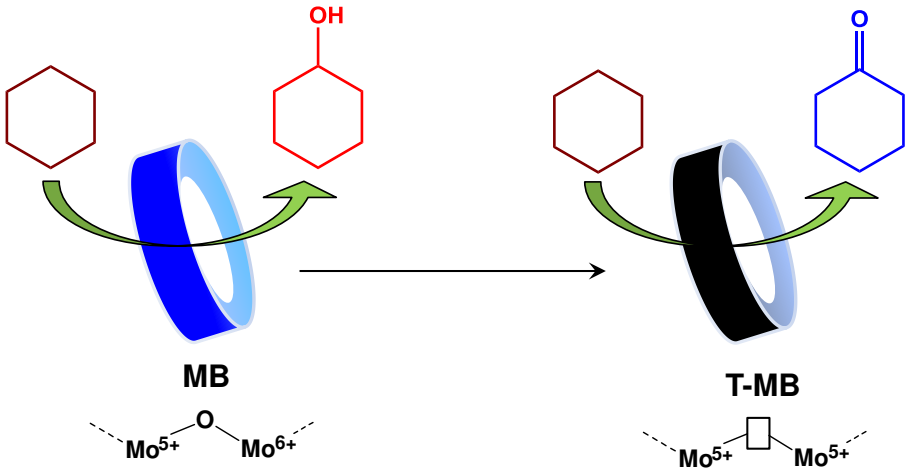

1 Introduction

Molybdenum blue (MB) is a polyoxometalate with a nanoring structure often used for colorimetric or quantification assays, particularly for phosphates, Si, V and W oxides, and sugars [1, 2]. Its structural characterization during the mid-1990s [3, 4], unveiled a stoichiometry comprising 154 Mo atoms forming a $[Mo^{VI}_{126}Mo^{V}_{28}O_{462}H_{14}(H_2O)_{70}]^{14-}$ anion, arranged in nanowheels of ca. 2 nm of internal diameter. This material gathered considerable attention in recent years as a model system for self-assembling inorganic structures [5, 6]. In fact, regular nanorings or clusters comprising 150 or 36 Mo units can be obtained from Na_2MoO_4 precursors [7].

A further feature of interest in this material is the presence of Mo^{5+}-O- Mo^{6+} units embedded into the nanoring structure [8], a property that we exploited showing that MB can be an efficient catalyst for the oxidation of cyclohexane [9]. In particular, MB had the interesting property to be is selective towards the formation of cyclohexanol rather than cyclohexanone and with minimal formation of adipic acid (the three major products of cyclohexane oxidation) [9]. Furthermore, this was achieved under reaction conditions (T = 140 ^{o}C, and P = 3 bar of O_2) that are similar to those industrially employed for the oxidation of cyclohexane using a cobalt naphthenate initiator [10]. As the conversion (ca. 6%) is also similar to that obtained from current industrial processes [11, 12], this makes MB a promising catalytic system for the oxidation of cyclohexane. Indeed, this is a crucial step for the manufacture of nylon fibres, with cylohexanol used as precursor for nylon-6,6 and cylohexanone as precursor for nylon-6. [13]

Current data suggest that for the oxidation of cyclohexane, MB is able to activate a true catalytic reaction pathway [9], rather than a promoted autoxidation as in the case of Co salts [14]. This prompted us to investigate the mechanistic features of this reaction in presence of MB and as a function of the amount of Mo^{5+}-O-Mo^{6+} bridges. In fact, by treating some metal oxides like MoO_3, WO_3, and Cr_2O_3 and high temperature (T > 180 ^{o}C) in the absence of oxygen, it is possible to remove lattice oxygen and this can affect their reactivity [15]. This procedure was also successfully employed in the gas phase oxidation of cyclohexane using MoO_3 without collapse of the metal oxide framework [16]. Therefore, this approach has been extended to remove lattice oxygen from MB and increase the amount of Mo^{5+}. The effect of this structural modification has been investigated in detail and a reaction mechanism for this catalyst, involving the decomposition of cyclohexyl hydroperoxide intermediate (C_6H_{11}-O_2H) is proposed.

2 Experimental

2.1 Synthesis of molybdenum blue

Molybdenum blue (MB) was prepared following with the procedure reported in [9] and references therein. Molybdenum metal powder (Sigma, assay 99.99% wt) was mixed with diluted hydrogen peroxide (Aldrich 30 wt%, trace metals < 10 ppm) and the suspension was stirred for 8 h at room temperature. The suspension was then filtered and the blue solid formed was dried using a rotary evaporator at room temperature in order to obtain a fine blue powder. Using such procedure, nanorings of ca. 3.8 nm external diameter [9] were obtained. Unlike other protocols, this procedure was deliberately used to minimize the presence of impurities and to have H^+ as counter ion rather than alkali metals.

2.2 Catalytic tests

Solvent-free oxidation of cyclohexane (Alfa Aesar, 8.5 g, HPLC grade) was carried out in a glass bench reactor using the desired amount of catalyst (6 mg). It should be noted that while MB is soluble in water, it is insoluble in cyclohexane; therefore we consider molybdenum as a heterogeneous catalyst under our reaction conditions. The reaction mixture was magnetically stirred at 140°C and 3 bar O_2 for 17 h. The reaction mixture was analysed by gas chromatography using a Varian 3200 gas chromatographer equipped with a CP-Wax 42 column. Acid products, such as adipic acid, were converted to their corresponding ester for quantification purposes [14]. An experimental error of 5% was determined for the quantification of the species in the reaction mixture, and this value as been used to compare the different catalytic tests in statistical terms.

2.3 Characterization of the catalyst

2.3.1 Diffuse reflectance spectroscopy

UV-Vis diffuse reflectance spectra were collected using a Harrick Praying Mantis cell mounted on a Varian Cary 4000 spectrophotometer. The spectra were collected from 850 to 200 nm at a scan speed of 60 nm min^{-1}. Background correction was carried out using Teflon powder (Spectralon). The sample was mounted on a 3 mm diameter diffuse reflectance sampling cup. Deconvolution analysis was carried out in the region 400-800 nm by means of Gaussian peaks [17]. The spectra were normalized to 1 unit of absorbance for comparison

purposes. The fitting of the spectra and their deconvolution was carried out using two procedures in order to provide a statistically univocal deconvolution set. A simplex algorithm [18] was used first to obtain an initial set of peak positions and peak widths, by a least absolute deviation analysis. This has the possible drawback of multiple solutions but it is more robust on outliers. The solution obtained by this regression was then used as input for a Levenberg-Marquardt algorithm [19] which operates on a least square curve fitting and provides a single fitting output. The fitting of the spectra was accepted when the fittings obtained using least absolute deviation analysis and least square fitting coincided within an error of the peak positions within 2 nm.

2.3.2 Solid State EPR

X-band continuous wave (CW) EPR spectra were recorded at room temperature in deoxygenated cyclohexane, using a Bruker EMX spectrometer. Typical instrument parameters were: centre field 3600 G, sweep width 800 G, sweep time 600 s, time constant 20 ms, power 1 mW, modulation frequency 100 kHz, and modulation width 5 G. EPR solid state spectra were collected at –133 ^{o}C (140 K) in a sealed quartz EPR tube.

A fresh MB sample for $^{17}O_2$ adsorption for solid state EPR was prepared in the following manner: the sample was inserted in a quartz EPR tube and treated under vacuum (40 mbar) for 8 h at 80 ^{o}C. This procedure was followed to remove oxygen from the gas phase before recording the spectrum at low temperature, in order to avoid dipolar broadening of the EPR line of the surface paramagnetic species caused by interaction with physisorbed molecular oxygen. The sample was then exposed to $^{17}O_2$ at room temperature and then the sample was further evacuated for 1.5h. The sample was then cooled at 140 K after this absorption for spectra recording.

2.4 EPR spin trapping

X-band continuous wave (CW) EPR spectra were recorded at room temperature in deoxygenated cyclohexane, using a Bruker EMX spectrometer. The typical instrument parameters were: centre field 3487 G, sweep width 100 G, sweep time 55 s, time constant 10 ms, power 5 mW, modulation frequency 100 kHz, and modulation width 1 G. Quantitative spectral analysis was carried out using WinSim software [20]. The spin trapping experiments were performed using the following procedure: 5,5-dimethyl-1-pyrroline N-oxide (DMPO) (0.1 mL of 0.1 M solution in cyclohexane) was added to the substrate (0.1 mL of 2.5 molar % solution of CHHP in cyclohexane), in an EPR sampling tube. The mixture was deoxygenated

by bubbling N_2 for 1 min prior to recording the EPR spectrum in order to enhance the signal [21]. Deoxygenation was carried out at room temperature 5 min after the mixing of the catalyst with the reaction mixture.

Cyclohexyl hydroperoxide (CHHP), was synthesized by a Grignard reagent-oxygen reaction, [22] and a solution of 2.5 mol% cyclohexyl hydroperoxide in cyclohexane was obtained.

3 Results and discussion

3.1 Thermal treatment of Molybdenum Blue

It was found that treating MoO_3 at temperatures above 180 ^oC in the absence of oxygen, removed oxygen from the lattice and this can affect its reactivity towards oxidation reactions involving hydrocarbons [16, 23]. The same procedure has been applied to MB with the aim to investigate the role of Mo^{5+} centres in the catalytic activity, as well as to prove the existence of an intermediate bound to the catalyst surface.

A thermally treated MB sample (here denoted as T-MB) was obtained from a fresh MB sample and treated at 180 ^oC for 48 h under flow of He (20 mL min^{-1}). Catalytic data for the oxidation of cyclohexane for a fresh a thermally treated MB samples are reported in table 1.

Table 1 Conversion and selectivity for a fresh (MB) and thermally treated MB (T-MB) sample for the oxidation of cyclohexane. Experimental conditions: catalysts 6 mg, cyclohexane 8.5 g, T = 140 ^oC and P = 3 bar O_2, reaction time = 17h. CHHP = cyclohexyl hydroperoxide.

Catalyst	Conversion (%)	Cyclohexanol	Cyclohexanone	CHHP	Adipic Acid	Selectivity (%) *
MB	6.0	52	40	0	1	93
T-MB	5.5	28	49	0	20	97

(*) total observed

Previous characterization of these materials by means of XRPD and HRTEM showed that the thermal treatment left the three-dimensional structure of the nanoring unaltered [9]. However, XPS data showed a change in the Mo^{5+}/Mo^{6+} ratio from 0.28 for MB, to 0.42 for T-MB, [9] thus presenting an increase in Mo^{5+} centres i.e. a reduction of the polyoxometalate as a consequence of oxygen removal from the MB lattice. This leads to a conversion that is statistically the same (that is within the experimental error of the GC method we used for the analysis of the reaction mixture) for the two materials, i.e. 6% conversion.), but the loss of selectivity to cyclohexanol (from 52 to 28%) from MB to T-MB.

3.1.1 DR-UV spectroscopy of Molybdenum Blue

In view of these characterization data, this prompted us to explore these two materials by means of other spectroscopic tools like diffuse reflectance-UV-Vis spectroscopy (DR-UV-Vis) and solid state EPR (SS-EPR). This with the aim to gather information on the electron hopping between Mo^{5+} and Mo^{6+} centres [24], as well as the local structure of these materials and possible binding modes of the oxygen to the MB nanoring (SS-EPR, section 3.1.2) [25].

UV-Vis spectra in the region between 400 and 800 nm for a fresh MB sample (Fig. 1), shows the clear presence of two bands at 611 and 659 nm, which are assigned to intervalence charge transfer (IVCT) bands [26], and the presence of a distinct shoulder at 450 nm.

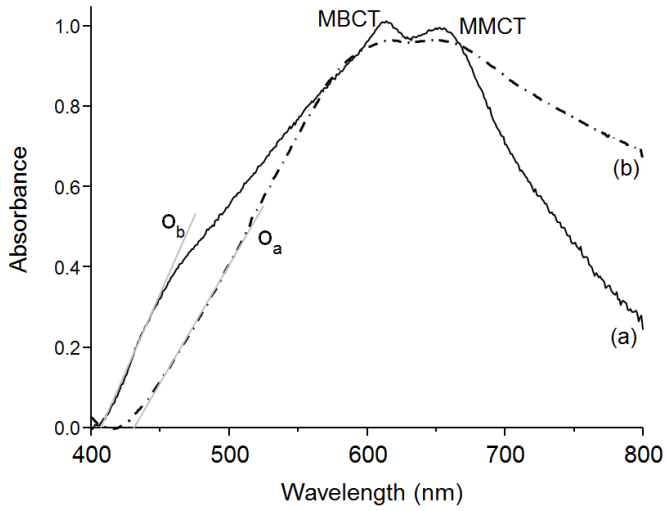

Fig. 1 DR-UV-Vis spectrum of: (a) fresh MB and (b) thermally treated T-MB sample. O_a and O_b refer to the offset for MB and T-MB respectively. A metal-to-bridge charge transfer (MBCT) band is detected at ca. 610 nm and a metal-to-metal charge transfer band is detected at ca. 650 nm (see table 3 for details).

Deconvolution of the MB UV-Vis spectrum using Gaussian peaks [17] (Fig. 2) lead to a fitting profile presenting six species (table 2). As MB presents a oxo-bridge system this gives rise to two intervalence bands [27], a band at high energy (low wavelength) due to a metal-to-bridge charge transfer (MBCT) [28] and a band at lower energy due to a metal-to-metal charge transfer (MMCT). This phenomenon has been observed in oxo-bridged Ru complexes [29], and we tentatively assign the peak at 611 nm to a MBCT band and the peak at 654 nm

to a MMCT band. For the shoulder at 450 nm instead, this leads to an offset of 410 nn and in turn a band gap [30] of 3.02 eV, a value very similar to the band gap of thin films of MoO_3 (3.04 eV) [31]. For the other three peaks/shoulders detected in figure 2, a full analysis of this spectrum would require a study of the excited states of MB [32], which is beyond the scope of the current manuscript. We do not consider the presence of six deconvolution peaks as a sign of a non-pure MB sample. In fact, XRPD [3] and SS-EPR (see section 3.1.2) show consistency with one MB species only. At present we can tentatively assign the bands at 494, 575 and 721 nm to localized oxygen ion vacancies [33] as observed for relatively known substoichiometric MoO_{3-x} [34]. However, this tentatively explanation is under debate [34] even for these materials, therefore much more work would be needed to determine and assign in full the several features that we are observing for MB. Yet this shows that MB is a highly complex system with several non-obvious features.

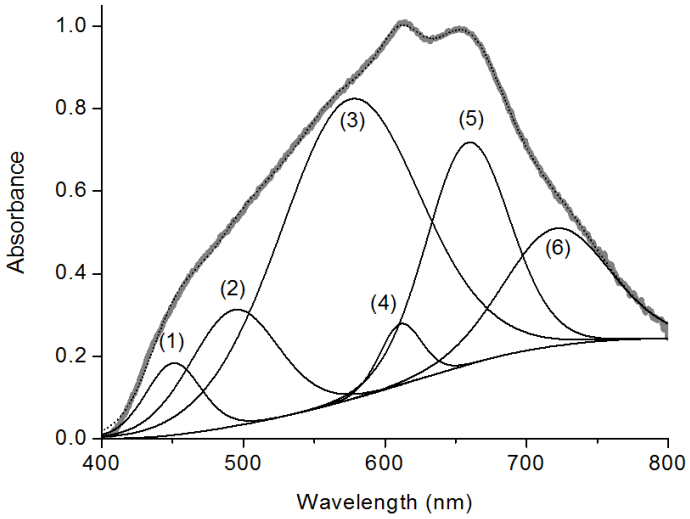

Fig. 2 Gaussian deconvolution for the DR-UV-Vis spectrum of fresh MB; (grey thick line) experimental spectrum; (black dotted line) simulated spectrum; six species labelled from (1) to (6) are identified (see table 3 for details).

For T-MB instead the DR-UV-Vis spectrum shows that the shoulder at 450 nm is lost, and the region at 600-660 nm now appears as two nearly unresolved bands with the peak at 611 nm almost disappearing, (figure 1 and 3) thus showing the disruption of the Mo^{5+}-O-Mo^{6+} moiety as a consequence of an increase in Mo^{5+} centres. By deconvolution of the T-MB UV-Vis spectrum, the most interesting feature is a strong reduction in the intensity of the signal at 612 nm (originally at 611 nm for the untreated sample, and with these two experimental

values identical within experimental error). This supports that our assignment for this band is indeed the due to a metal-to-bridge charge transfer process. In fact, as oxygen is removed from the lattice the bridge is disrupted and in turn the intensity of its signal.

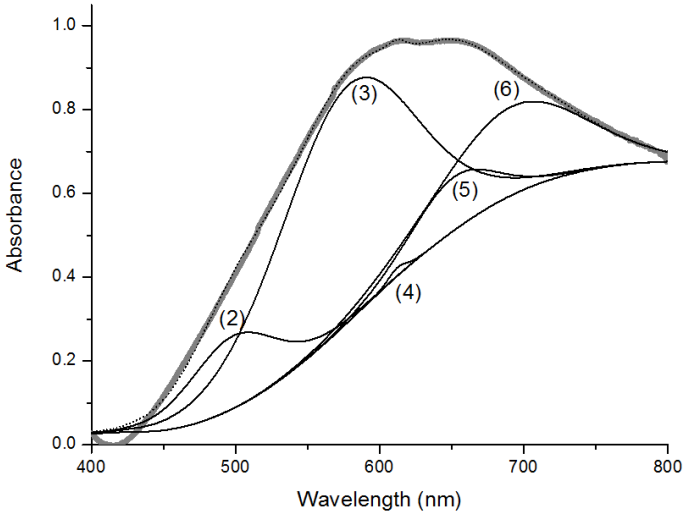

Fig. 3 Gaussian deconvolution for the DR-UV-Vis spectrum of T-MB; (grey thick line) experimental spectrum; (black dotted line) simulated spectrum; five species are identified, a numbering from (2) to (5) is used to preserve the labelling of the species reported in Fig. 2 (see table 3 for details).

Furthermore, the loss of the shoulder at 450 nm leads now to an offset of ca. 430 nm i.e. a band gap of 2.88 eV. This is a lower value compared to fresh MB and further consistent with oxygen removal from the lattice [35], yet without a collapse of the 3D framework of the nanoring structure [9].

Table 2 Band position summary for MB and T-MB after gaussian deconvolution. The labelling from (1) to (6) refers to figures 2 and 3.

Band from deconvolution	**MB λ_{max} (nm)**	**T-MB λ_{max} (nm)**
(1)	450	n.d.
(2)	494	498
(3)	575	577
(4)	611	612
(5)	659	651
(6)	721	691

3.1.2 Solid state EPR spectroscopy of MB and T-MB

Due the presence of Mo^{5+} centres in MB, and to gather additional structural information on this material, we considered the use of solid state EPR (SS-EPR). Mo^{5+} is EPR active (electron configuration [Kr] $4d^1$) and with an expected hyperfine structure presenting six EPR

signals due to the interaction between the unpaired electron and the nuclear spin (I = 5/2) of the isotopes ^{95}Mo and ^{97}Mo [36]. However, a solid state EPR spectrum of MB collected at 140 K (Fig. 4) showed four peaks only. This is a consequence of the large amount of Mo^{5+} centres in our sample, which are also constrained in a nanoring of external diameter of ca. 3.8 nm [3, 9]. The combination of these two factors make the Mo^{5+} paramagnetic centres not isolated each other, thus leading to dipolar coupling interaction [37] and in turn to line broadening and unresolved spectra.

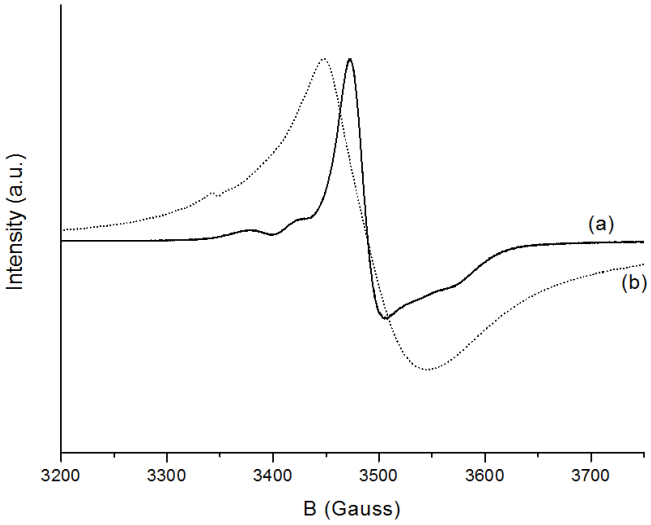

Fig. 4 Solid state EPR spectrum at 140K of: (a) fresh MB sample, and (b) thermally treated T-MB sample, (the spectra have been scaled to the same intensity in order to better appreciate the difference in line broadening between these two samples).

SS-EPR spectroscopy for a T-MB sample was also carried out, but the resulting spectrum was even broader and with less features than fresh MB. Considering the results obtained by DR-UV-Vis, (section 3.1.1) and previous XPS data [9] we conclude that the broadening effect that we observe in this EPR spectrum, is due to an increase in Mo^{5+} concentration only; and not by an extensive antiferromagnetic coupling followed by collisions of the paramagnetic centres with oxygen [38].

Despite this non-informative result, and yet the role of oxygen in driving the selectivity to a desired oxidation product as a function of the MB electronic structure, we collected EPR spectra of MB in presence of $^{17}O_2$. In fact, the binding mode of O_2 to a Mo centre could in principle be detected by SS-EPR at low temperature [39], with discrimination between O_2 adsorption modes to a metal centre. For example just one oxygen atom bound to a metal, or a binding mode via both the O atoms to a metal centre. To promote O_2 adsorption, a fresh MB sample was treated under vacuum overnight at 140 ^{o}C and then exposed to a $^{17}O_2$ atmosphere (figure 5). However, also in this case no signal from $^{17}O_2$ was detected (expected signal

between 3400 and 3500 G, with our centre field, for adsorbed $^{17}O_2$; and between 3600-3700 G for changes in coordination of Mo [25]). Even if the catalytic properties of MB originate from the presence of Mo^{5+} centres, it appears that is precisely the large amount of these species that prevents also the identification of any $^{17}O_2$ hyperfine structure over the MB surface. This further shows, as for DR-UV-Vis, that MB is a challenging system to study due to the inner complexity of its electronic structure.

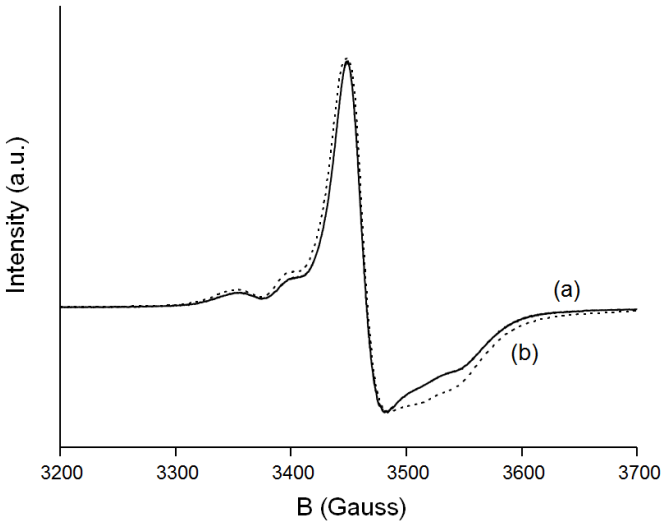

Fig. 5 Solid state EPR spectrum at 140 K of: (a) fresh MB and (b) MB after exposure to $^{17}O_2$.

3.2 Nature of the oxidation reaction of cyclohexane in presence of MB, and CHHP decomposition

As a consequence of the results we have observed in this study, and with the aim of finding a correlation between a change in electronic properties of MB and the product distribution, the oxidation reaction of cyclohexane was investigated using EPR spin trapping methodology (see section 3.2.1).

However, in our case these experiments were not directly carried out for the oxidation of cyclohexane, but rather for the decomposition of cyclohexyl hydroperoxide (CHHP). This for two reasons: (i) CHHP is considered a key intermediate of the oxidation process (vide infra) and (ii) intrinsic pressure and temperature limitations to carry out spin trapping experiments at 140 ^{o}C and 3 bar. Despite these apparent constraints, useful information can obtained in order to gather information on the reaction mechanism for the oxidation of cyclohexane catalysed by MB (section 3.3). In fact, there is a crucial point that emerges from the analysis of the product distribution. Liquid phase oxidations may occur via a true catalytic process, or

by means of autoxidation [40] that is an unselective oxidation route where the selectivity is purely dictated by the reactivity of free radicals in solution and not by the catalyst.

Due to its importance for our study, the accepted reaction pathway for autoxidation is reported here, as well as how MB can modify it. The classical scheme of homolytic oxygen activation for the autoxidation of hydrocarbons is given in equations 1-4 [41], where I* is any species capable to abstract an H atom from the reagent C_6H1_2.

$$I^* + C_6H_{11}\text{-}H \rightarrow I^*\text{-}H + C_6H_{11}\cdot \quad \text{(eq. 1)}$$

$$C_6H_{11}\cdot + O_2 \rightarrow C_6H_{11}O_2\cdot \quad \text{(eq. 2)}$$

$$C_6H_{11}O_2\cdot + C_6H_{11}\text{-}H \rightarrow C_6H_{11}\text{-}O_2H + C_6H_{11}\cdot \quad \text{(eq. 3)}$$

$$C_6H_{11}\text{-}O_2H + C_6H_{11}\text{-}O_2H \rightarrow C_6H_{10}{=}O + C_6H_{11}\text{-}OH + O_2 \quad \text{(eq. 4)}$$

This scheme is usually subdivided in: initiation (eq. 1), propagation (eqs. 2-3) and termination (eq. 4). In this scheme $C_6H_{11}O_2\cdot$ is the chain carrier of this free radical pathway process (eq. 3), and CHHP ($C_6H_{11}\text{-}O_2H$) is involved in the propagation and formation of the products (eqs. 3-4) [41]. It should be noted that if this mechanism is operating without any selectivity control by a catalytic surface, or even radical scavengers, the expected ratio of ketone to alcohol should be 1:1 (eq. 4).

However, the ketone can also be obtained via H_α abstraction by the chain carrier $C_6H_{11}O_2\cdot$ in a pathway that is still operating via a pure free radical pathway [38] (eqs. 5-6):

$$C_6H_{11}\text{-}O_2\cdot + C_6H_{11}\text{-}O_2H \rightarrow C_6H_{11}\text{-}O_2H + C_6H_{10}(\cdot)\text{-}O_2H \quad \text{(eq. 5)}$$

$$C_6H_{10}(\cdot)\text{-}O_2H \rightarrow C_6H_{10}{=}O + \cdot OH \quad \text{(eq. 6)}$$

On the other hand, by thermal effect, or by the presence of an active metal centre, CHHP decomposition may also occur [43]:

$$C_6H_{11}\text{-}O_2H \rightarrow C_6H_{11}\text{-}O\cdot + \cdot OH \quad \text{(eq. 7)}$$

with the alkoxyl radical reacting with a cyclohexane molecule to form the alcohol:

$$C_6H_{11}\text{-}O\cdot + C_6H_{12} \rightarrow C_6H_{11}\text{-}OH + C_6H_{11}\cdot \quad \text{(eq. 8)}$$

In this case, if equations 7-8 are kinetically dominant with respect to equations 5-6, this would lead to an excess of alcohol with respect to the ketone instead. That is why the investigation of the decomposition of CHHP is important in the current study.
It does also worth noting, that CHHP decomposition is also at the centre of the cyclohexane oxidation by cobalt salts, as carried out in industrial context [10]. In this case, it is accepted that a Haber-Weiss cycle is operating in agreement with the scheme [44]:

$R\text{-}O_2H + Co^{II} \rightarrow Co^{III}\text{-}OH + RO\cdot$ (eq. 9)

$Co^{III}\text{-}OH + R\text{-}O_2H \rightarrow Co^{II} + RO_2\cdot + H_2O$ (eq. 10)

Net equation:

$2\ R\text{-}O_2H \rightarrow RO_2\cdot + RO\cdot + H_2O$ (eq. 11)

However, systems operating on the principle of cobalt salts, usually have a ketone to alcohol ratio (K/A ratio) in the range of 1.5, [14, 45], whereas in our case it is the alcohol to be in excess, (K/A = 0.8 for fresh MB), thus suggesting a dominance of equations 7 and 8, i.e. a fast homolytic CHHP decomposition by MB.

Therefore we consider CHHP a key intermediate in our catalytic process, and more in detail with CHHP adsorbed over MB surface during the oxidation reaction. In fact, in our case the thermal treatment of the catalyst removes oxygen at the expenses of the Mo^{5+}-O-Mo^{6+} moiety to increase the amount of Mo^{5+} centres (but still preserving the nanoring structure). As shown in sections 3.1 the conversion is preserved, but the selectivity to the alcohol is lost, thus showing that the selectivity we observe is a consequence of the chemical nature of the catalyst. In fact, if this should not be the case, and the reaction to be a pure liquid phase autoxidation process, i.e. without any adsorbed intermediate species, we should then detect the same selectivity for MB and T-MB, with the product distribution dictated by a pure free radical chain autoxidation process only. In contrast, because the selectivity is different for fresh MB and thermally treated T-MB, this means that one of the intermediates of the reaction has to be bound to surface of the MB, and thus the reaction is truly heterogeneously catalysed. A similar effect has been recently observed for cobalt silicates, where an enhanced selectivity to the ketone was observed instead as a function of the amount of Co^{2+} centres [46]. Due to our experimental conditions we cannot yet directly detect CHHP adsorbed over MB (i.e. a very dispersed catalyst in liquid phase, and at high temperature and pressure). Still

CHHP is an intermediate that can drive the selectivity to the alcohol [46], and it is for these combined reasons that we carried out spin trapping experiments on this species in order to identify the mechanism for this reaction.

3.2.1 EPR Spin trapping for the CHHP decomposition by fresh and thermally treated MB

The principle of the spin-trapping methodology relies on the fast selective addition, i.e. trapping, of short-lived radicals to a diamagnetic spin trap, usually a nitrone or a nitroso compound, such as 5,5-dimethyl-1-pyrroline-N-oxide (DMPO). The result of this addition, known as spin adduct, is a persistent free nitroxide radical with a sufficiently long lifetime to enable detection by conventional EPR spectroscopy [47]. Hyperfine coupling constants between the unpaired electron in the spin adduct and the hydrogen in the beta position of DMPO (Fig. 6, top) where calculated. Thus it was possible to assign the structure of the original short-lived radicals [48]. Spin trapping spectra, and their deconvolution, for the decomposition of CHHP by MB and T-MB are reported in figures 6 and 7 respectively. The simulation of the spectra led to assign the following species: a di-tert-butyl-nitroxide derivative [49], a DMPO-O-C_6H_{11} [50], and a DMPO-O_2-C_6H_{11} spin adduct [51] a DMPO-C_6H_{11} carbon-centred adduct characteristic of the parent radical C_6H_{11}• [52] and a carbon centred adduct which is possibly a DMPO-C(OH)R_2 [53].

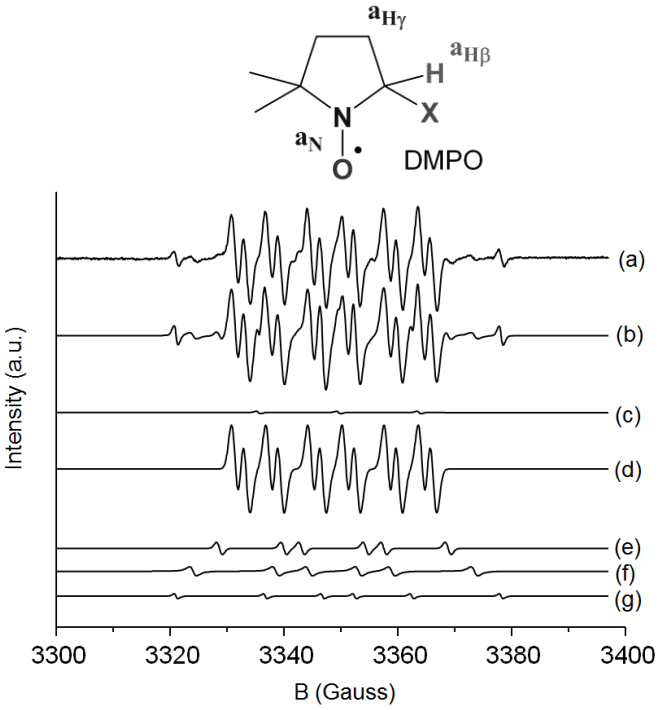

Fig. 6 (top) DMPO structure and coupling constants for simulation of the spectra; (bottom) deconvoluted EPR spectra of DMPO spin adducts obtained during the decomposition of CHHP in cyclohexane in the presence of MB: (a) experimental spectrum and (b) simulated spectrum; (c) di-tert-butyl-nitroxide derivative, (d) DMPO-O-C_6H_{11} spin adduct, (e) DMPO-O_2-C_6H_{11} adduct, (f) DMPO-C_6H_{11} carbon centred adduct, and (g) carbon centred adduct, which is possibly a DMPO-C(OH)R_2 species.

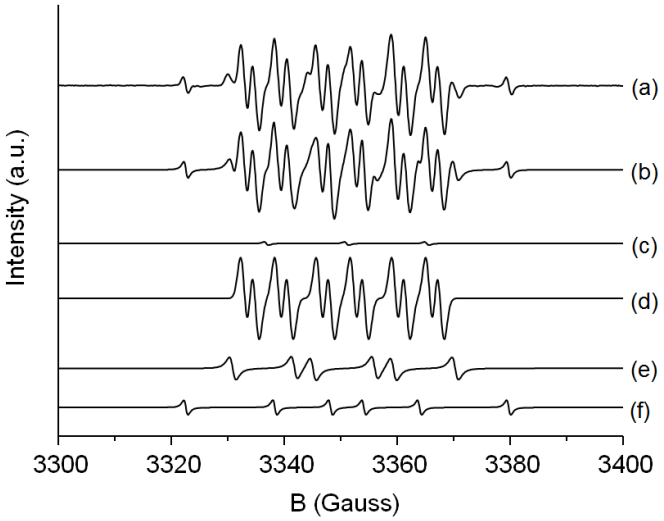

Fig. 7. Deconvoluted EPR spectra of DMPO spin adducts obtained during the decomposition of CHHP in cyclohexane in the presence of thermally treated T-MB: (a) experimental spectrum and (b) simulated spectrum; (c) di-tert-butyl-nitroxide derivative, (d) DMPO-O-C_6H_{11} spin adduct, (e) DMPO-O_2-C_6H_{11} adduct, and (f) carbon centred adduct, which is possibly a DMPO-C(OH)R_2 species.

Spectra simulation for MB and T-MB, led to the spin Hamiltonian parameters reported in table 3. Moreover, as the line broadening of the two EPR spin trapping spectra for MB and T-MB is the same, this allows a comparison of the relative amounts of species that have been trapped. However, it should be underlined that the spin trapping technique only allows for semi-quantitative determination of the detected adducts. This is a consequence of the life-time of the spin adduct, the nature of the solvent, the temperature as well as the efficiency of the capture reaction which is different for each radical [54]. Yet considering these limitations, a quantification of the relative amount of spin adducts is possible and was carried out (table 3) with the aim to estimate differences in peroxyl and alkoxyl radicals concentration for MB and T-MB.

Table 3. Coupling constants of DMPO spin adducts for the CHHP decomposition in cyclohexane by MB and T-MB at room temperature (thermally treated values in bracket, n.d. = not detected)

Radical	**a_N (G)**	**$a_{H(\beta)}$ (G)**	**$a_{H(\gamma)}$ (G)**	**Amount of adducts (%)**

	MB	T-MB	MB	T-MB	MB	T-MB	MB	T-MB
nitroxide derivative	14.20	14.22					2.2	0.9
C_6H_{11}-O•	13.36	13.40	6.02	6.01	1.90	1.90	83	71
C_6H_{11}-OO•	14.23	14.44	10.92(*)	11.46(*)			6.2	21
C_6H_{11}•	14.56	n.d.	20.46	n.d.			4.1	n.d.
R_2(OH)C•	15.75	15.67	25.61	25.67			4.5	7.1

(*) this difference in coupling constant is not considered significant, and the two adducts can be considered the same in both cases.

From these data T-MB presents a lesser amount (ca. 71%) of alkoxyl spin adduct radical if compared to fresh MB (ca. 83%), and it also exhibits a much larger amount of peroxyl adduct (by a factor of ca. 3) compared to fresh MB. These data well match with the reduced selectivity to cyclohexanol that is observed for T-MB, and in turn confirm the pivotal role of CHHP as intermediate for the formation of cyclohexanol for fresh MB. By comparison, studies on the sole autoxidation of cyclohexane in the absence of any catalysts showed an amount of DMPO-O-C_6H_{11} radical adducts of 50% and peroxyl radical adducts of DMPO-O_2-C_6H_{11} of ca. 43% [55] and a K/A ratio close to 1. Assuming a similar efficiency for the spin trapping reaction from DMPO between these studies, the current set of data shows a higher amount of C_6H_{11}-O• species in solution when MB is used together with more alcohol.
Two further interesting features for the relative amount of spin adducts are observed when T-MB is used: (i) a total disappearance of C_6H_{11}• parent radical, and (ii) an increased amount of R_2(OH)C• adduct. As the latter species (R_2(OH)C•) is likely to be a ring opening product [56], this could link to adipic acid formation [57]. It is interesting to observe how the amount of adipic acid is much higher for the thermally treated sample T-MB (ca. 20%) (table 1), and nearly absent for fresh MB. This would provide a further match for the data we collected, thus allowing to correlate spin trapping tests and the catalytic results. This is an important aspect as the catalytic tests were carried out at 140 ^{o}C and 3 bar of O_2, whereas the EPR experiments were carried out at room temperature and atmospheric pressure.

3.3 Proposed reaction scheme for the oxidation of cyclohexane by MB

In view of these results, i.e. : (i) decomposition of CHHP by MB, (ii) existence of a Mo^{5+}-O-Mo^{6+} moiety as a centre of the catalytic activity, and an (iii) enhanced selectivity of MB

towards cyclohexanol; we propose a reaction scheme for the cyclohexanol formation (Scheme 1):

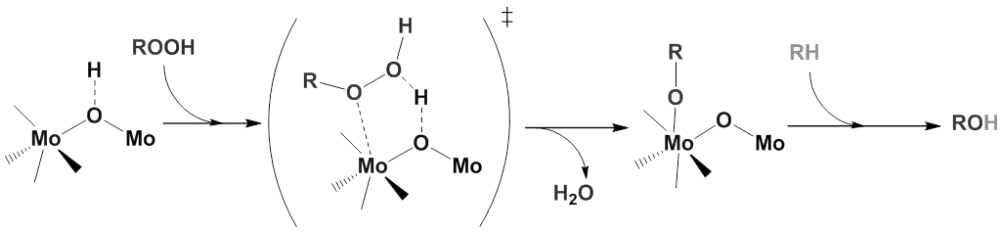

Scheme 1 Postulated reaction mechanism for the formation of cyclohexanol in the oxidation of cyclohexane via a CHHP intermediate catalysed by MB (for simplicity a fragment of MB only is considered in this scheme, and charges are also neglected)

It should also be noted that in this scheme we make explicit use of a H^+ centre (for simplicity charges are omitted). This because H^+ species are present in the stoichiometry of the MB that we synthesised as counter ion of the Mo nanowheel $14H^+ \cdot [Mo^{VI}_{126}Mo^{V}_{28}O_{462}H_{14}(H_2O)_{70}]^{14-}$. In this scheme CHHP (ROOH) adsorbs over a Mo-O-Mo moiety or over a MoO(H)Mo unit. This results in the cleavage of the O-O bond of CHHP and elimination of a water molecule. An alkoxy radical (RO•) remains adsorbed to a Mo centre, then by the presence of a proximal C_6H_{12} molecule (please note the reaction is carried out under solvent-free conditions) a H-abstraction reaction occurs, with the formation of cyclohexanol and a parent radical C_6H_{11}•. This parent radical then reacts with molecular oxygen under diffusion limitation control [60] to form a C_6H_{11}-O_2• species, which by further reaction with C_6H_{12} will form CHHP and so on, to be a chain carrier for the catalytic cycle.

We would also like to stress the analogies of this mechanism with the cyclohexane oxidation by Mn-AlPO-5 catalysts developed by Iglesia and co-workers [61], where these materials showed enhanced selectivity to the alcohol, as well as decomposition of CHHP as a key intermediate for the oxidation process. In our case though we do not consider the adsorption of O_2 to MB as a possible reaction pathway (either as parallel or predominant route), like proposed for AlPO catalysts. In fact, if we compare the adsorption rate of O_2 to a MoO_x surface in solution, to the reaction rate of C_6H_{11}• with molecular O_2 in solution, the latter is basically a energetically barrierless process limited by diffusion only [60]. This fact, added to the minimal amount of MB used in our catalytic tests (metal to substrate molar ratio 1: $5.4 \cdot 10^7$), lead us to conclude that in our case molecular O_2 adsorbed over MB (if any) is most likely not responsible for the catalytic cycle. And it is the molecular oxygen that is in solution that takes part to the reaction instead.

4. Conclusions

MB is a polyoxometalate capable of catalytic oxidation of cyclohexane to cyclohexanol as major product. A key feature of the catalytic activity of MB is its electronic structure comprising a Mo^{5+}-O-Mo^{6+} moiety. DR-UV-Vis data analysis revealed a complex electronic structure, with electron hopping between Mo^{5+} and Mo^{6+} centres via the oxygen bridge. By removing lattice oxygen from MB via thermal treatment (T-MB), this increased the amount of Mo^{5+} into the catalyst, disrupting the Mo^{5+}-O-Mo^{6+} linkage, but leaving the framework of the nano-ring structure basically unmodified. If T-MB was used for the oxidation of cyclohexane and compared with a fresh (thermally untreated) MB sample, the conversion was basically the same for both of these materials; however the selectivity was substantially altered. T-MB decreased the selectivity to the alcohol (the major product for fresh MB), and led to a large formation of adipic acid (which was nearly absent for fresh MB).

The presence of a high amount of Mo^{5+} centres in both MB and T-MB appears to be at the heart of the catalytic activity for these materials, yet it precluded the analysis of oxygen species over the catalyst surface, and in turn the direct detection of an intermediate over the catalyst surface. Nevertheless, we can deduce that an intermediate (CHHP in our case), has to be bound over the MB surface. In fact, if this should not happen, the reaction would just be a liquid phase autoxidation initiated by any Mo centre, and the product selectivity would be expected to be the same for both MB and T-MB. However, the catalytic tests show otherwise. In addition, by using EPR spin trapping experiments we showed that CHHP is involved in the oxidation process of cyclohexane, and it is possible to correlate this intermediate to the formation of cyclohexanol when MB is used. This allowed us to propose a reaction mechanism in which CHHP is adsorbed over the catalyst surface in analogy with AlPO catalysts [55], but with molecular oxygen that reacts with C_6H_{11}• radicals in liquid phase via a diffusion limited route, rather than to be adsorbed over the catalyst surface.

Acknowledgements

The authors wish to acknowledge the support of INVISTA Textiles (UK) Limited, INVISTA Intermediates and INVISTA Technologies S. à r. l.

References

1. He Z, Honeycutt C (2005) Commun Soil Sci Plan 36:1373
2. Deng SP, Tabatabai MA (1994) Soil Biol Biochem 26:473
3. Müller A, Meyer J, Krickemeyer E, Diemann E (1996) Angew Chem Int Ed 35:1206
4. Müller A, Serain C (2000) Acc Chem Res 33:2
5. Xuan W, Surman AJ, Miras HN, Long DL, Cronin L (2014) J Am Chem Soc 136:14114
6. Long DL, Tsunashima R, Cronin L (2010) Angew Chem Int Ed 49:1736
7. Miras HM, Richmond CJ, Long DL, Cronin L (2012) J Am Chem Soc 134:3816
8. Zhong D, Sousa FL, Müller A, Chi L, Fuchs H (2011) Angew Chem Int Ed 50:7018
9. Liu X, Conte M, Weng W, He Q, Jenkins RL, Watanabe M, Knight DW, Murphy DM, Whiston K, Kiely CJ, Hutchings GJ (2015) Catal Sci Technol 5:217
10. Vanoppen DL, De Vos DE, Genet MJ, Rouxhet PG, Jacobs PA (1995) Angew Chem Int Ed 34:560
11. Guo CC, Chu MF, Liu Q, Liu Y, Guo DC, Liu XQ (2003) Appl Catal A 246:303
12. Kumar R, Sithambaram S, Suib SL (2009) J Catal 262:304
13. Dapurkar SE, Sakthivel A, Selvam P (2004) J Mol Catal A Chem 223:241
14. Hereijgers BPC, Weckhuysen BM (2010) J Catal 270:16
15. Ressler T, Walter A, Huang ZD, Bensch W (2008) J Catal 254:170
16. Conte M, Chechik V (2010) Chem Commun 46:3991
17. Langhals H (2000) Spectrochim Acta A 56:2207
18. Leandri R (2001) J. Chemometrics 15: 559
19. Alper JS, Gelb RI (1990) J Phys Chem 94:4741
20. Simulations were carried out using WinSim software: http://www.niehs.nih.gov/research/resources/software/tox-pharm/tools/index.cfm.
21. Conte M, Ma Y, Loyns C, Price P, Rippon D, Chechik V (2009) Org Biomol Chem 7:2685
22. Walling C, Buckler SA (1955) J Am Chem Soc 77:6032
23. Labanowska M (1999) Phys Chem Chem Phys 1:5385
24. Qiu H, Xu T, Wang Z, Ren W, Nan H, Ni Z, Chen Q, Yuan S, Miao F, Song F, Long G, Shi Y, Sun L, Wang J, Wang X (2013) Nat Commun 4:2642
25. Dyrek K, Che M, (19970 Chem Rev 97:305
26. Bugayev AA, Nikitin SE (2000) Opt Commun 180:69
27. Glover SD, Kubiak CP (2011) J Am Chem Soc 133:8721

28. Brunschwig BS, Creutz C, Sutin N (2000) Chem Soc Rev 31:168
29. Canzi G, Goeltz JC, Henderson JS, Park RE, Maruggi C, Kubiak CP (2014) J Am Chem Soc 136:1710
30. Chithambararaj A, Sanjini NS, Velmathi S, Bose AC (2013) Phys Chem Chem Phys 15:14761
31. Hussain Z (2001) J Mater Res 16:2695
32. Uemura T, Ohba M, Kitagawa S (2004) Inorg Chem 43:7339
33. He T, Yao J (2003) J Photochem Photobiol C 4:125
34. Chudnovskii FA, Schaefer DM, Gavrilyuk AI, Reifenberger R (1992) Appl Surf Sci 62:145
35. Ganduglia-Pirovano MV, Hofmann A, Sauer J (2007) Surf Sci Rep 62:219
36. Torok B, Torok M, Rozsa-Tarjani M, Palinko I, Horvath LI, Kiricsi I, Molnar A (2000) Inorg Chim Acta 298:77
37. Catoire B (Ed.) (1992) Electron Spin Resonance (ESR) Applications in Organic and Bioorganic Materials, Springer-Verlag Berlin, Heidelberg, p.190
38. Berliner L (Ed.) (2003) In Vivo EPR (ESR): Theory and Application in Biologic Magnetic resonance, Kluwr/Plenum publishers, New York, p.442
39. Chiesa M, Giamello E, Che M (2010) Chem Rev 110:1320
40. Liu X, Ryabenkova Y, Conte M (2015) Phys Chem Chem Phys 17:715
41. Partenheimer W (1995) Catal Today 23:69
42. Hermans I, Jacobs PA, Peeters J (2006) Chem Eur J 12:4229
43. Weinstein J, Bielski BHJ (1979) J Am Chem Soc 101:58
44. Tanase S, Bouwman E, Reedijk J (2004) Appl Catal A 259:101
45. Ramanathan A, Hamdy MS, Parton R, Maschmeyer T, Jansen JC, Hanefeld U (2009) Appl Catal A 355:78
46. Hmady MS, RamanathanA, Maschmeyer T, Hanefled U, Jansen JC (2006) Chem Eur J 12:1782
47. Conte M, Miyamura H, Kobayashi S, Chechik V (2009) J Am Chem Soc 131:7189
48. Conte M, Wilson K, Chechik V (2007) Org Biomol Chem 7:1361
49. Novak M, Brodeur BA (1984) J Org Chem 49:1142
50. Baum SL, Anderson IGM, Baker RR, Murphy DM, Rowlands CC (2003) Anal Chim Acta 481:1
51. Davies MJ, Slater TF (1986) Biochem J 240:789
52. Janzen EG, Evans CA, Liu JP (1973) J Magn ResoN 9:513

53. Conte M, Wilson K, Chechik V (2010) Rev Sci Instrum 81:104102
54. Ionita P, Conte M, Gilbert BC, Chechik V (2007) Org Biomol Chem 5:3504
55. Conte M, Liu X, Murphy DM, Whiston K, Hutchings GJ (2012) Phys Chem Chem Phys 14:16279
56. Silke EJ, Pitz WJ, Westbrook CK, Ribaucour M (2007) J Phys Chem A 111:3761
57. Lee SO, Raja R, Harris KDM, Meurig Thomas J, Brian BFG, Sankar G (2003) Angew Chem Int Ed 42:1520
58. Jensen RK, Korcek S, Mahoney LR, Zinbo M (1981) J Am Chem Soc 103:1742
59. Modén B, Zhan BZ, Dakka J, Santiesteban JG, Iglesia E (2006) J Catal 239:390
60. Stark MS (2002) J Am Chem Soc 122:4162